buildings

MDPI

Article

Regulating Hydration Heat in Magnesium Phosphate Cement Using Paraffins: Efficacy and Performance Trade-Offs

Zhenxiang Lin [1], Haoyang Jiang [1], Hansong Zhang [1], Jie Liu [1], Xiaoying Liu [1], Junyu Fan [2] and Zhide Hu [1,*]

[1] Department of Military Facilities, PLA Joint Logistic Support Force University of Engineering, Chongqing 401331, China; xavierlin0725@163.com (Z.L.); jianghywangyi@163.com (H.J.); zhanghs227@hotmail.com (H.Z.); liujiely@hotmail.com (J.L.); lxy_ctbu@163.com (X.L.)

[2] National Engineering Research Center for Disaster and Emergency Rescue Equipment, Chongqing 401331, China; ssdfanjunyu@gmail.com

* Correspondence: huzd6503@163.com

Abstract

Magnesium phosphate cement (MPC) holds great potential for rapid repairs, yet its practical application is limited by its intense hydration exotherm. While many existing studies confirm paraffin (PA)'s ability to regulate hydration heat in other cement-based materials, the comparison of hydration heat regulation efficacy among PAs with different phase change temperatures and the accompanying performance trade-offs in MPC systems remain insufficiently explored. This study comprehensively evaluates the effects of three PAs with distinct phase change characteristics (n-C18, n-C20, n-C22) and their contents on the hydration heat regulation and performance of MPC. Direct incorporation of PAs was adopted to assess its practical feasibility, considering construction cost-effectiveness. Investigations were conducted using hydration heat release tests, temperature rise monitoring, DSC, mechanical tests, XRD, and SEM. Results show that all PAs significantly retarded heat release and suppressed temperature rise, with efficacy increasing with phase change temperature; a maximum exothermic peak reduction of 64% was achieved with 4% n-C22. PAs also introduced distinct temperature plateaus near their phase change temperature, further enhancing temperature regulation. As a key trade-off, compressive strength decreased with increasing PA content, but mixtures with n-C18 $\leq$ 8%, n-C22 $\leq$ 4%, and n-C20 = 2% still met the standard strength requirement for rapid repair, 3 h compressive strength $\geq$ 20 MPa. Microstructural analysis reveals that while regulating hydration heat, PA also hindered the hydration product formation and crystallization, underpinning the observed performance trade-offs. This study establishes a clear performance correlation between PAs with different phase change temperatures and MPC, clarifies the intrinsic trade-offs between heat regulation and mechanical properties, and offers actionable guidance for engineering applications—facilitating the development of high-performance PA/MPC composites with controllable heat release for rapid repair scenarios.

Keywords: magnesium phosphate cement; paraffin; phase change materials; hydration heat; compressive strength; performance trade-off

Check for updates

Academic Editor: Flavio Stochino

Received: 9 December 2025
Revised: 6 January 2026
Accepted: 8 January 2026
Published: 11 January 2026

Copyright: © 2026 by the authors. Licensee MDPI, Basel, Switzerland. This article is an open access article distributed under the terms and conditions of the Creative Commons Attribution (CC BY) license.

1. Introduction

Magnesium phosphate cement (MPC) is a high-strength cementitious material, produced by the acid–base reaction among dead burned magnesium oxide (dead burned MgO), soluble phosphates, retarders, and modifying agents in specific proportions. MPC combines the advantages of cement, ceramics, and refractory materials, featuring excellent

plasticity, rapid setting, high early strength, low-temperature hardening capability, superior bond compatibility, high refractoriness, and strong resistance to seawater corrosion [1–4]. These characteristics make MPC highly suitable for applications such as rapid repairs and emergency military construction, particularly in challenging projects like island and reef expansion [5–7]. However, the widespread application of MPC is constrained by its intense hydration exothermic behaviour. Specifically, the intense heat release not only accelerates setting and shortens the operable time for construction but also induces significant thermal gradients due to concentrated heat release and high peak temperatures, resulting in cracking, deformation, and energy waste [1,8–13].

Phase change materials (PCMs) have emerged as a promising strategy for hydration heat regulation in cementitious systems [14–17], as they can absorb or release substantial amounts of latent heat during phase change near a specific temperature, with the temperature remaining relatively stable [18–20]. Leveraging high energy storage density and reversible melting-solidification cycles, PCMs have been incorporated into cement-based materials to mitigate hydration heat and impart thermal energy storage functionality [21–26]. Among common PCMs, paraffin (PA) is particularly attractive due to its non-corrosiveness, chemical inertness, negligible supercooling, and good cyclic stability [27,28]. With a latent heat exceeding 200 J/g, PA has been widely used in phase change cement-based composites [10,29–32]. Given the intense hydration exothermic behaviour of MPC, PCMs such as PA have shown great potential for regulating the MPC hydration heat. However, while some MPC studies have reported enhanced strength or prolonged setting time with PCMs [13,33,34], a more common observation is the non-negligible trade-offs between hydration heat regulation and performance [35–38]. As linear alkanes (C_nH_{2n+2}), PA's phase change temperature and enthalpy are dictated by its carbon chain length, suggesting that PAs could impart different regulatory effects on hydration heat [39–41]. Notably, existing studies have predominantly focused on a single type of PA or fixed composite formulations, lacking systematic comparisons of hydration heat regulation efficacy and in-depth assessment of performance trade-offs among PAs with distinct phase change temperatures—especially in the MPC system.

To address that, the present study systematically evaluates the effects of three PAs—n-octadecane (n-C18), n-eicosane (n-C20), and n-docosane (n-C22)—on hydration heat regulation and the performance of MPC. The direct incorporation method was adopted for its cost-effectiveness to evaluate its practical feasibility [10,42,43]. Despite potential limitations such as PA leakage and strength reduction, this work aims to provide a comparative analysis of the hydration heat regulation efficacy of different PAs and to clarify the resulting performance trade-offs, which is essential before advancing to more complex encapsulation strategies. By comprehensively evaluating hydration heat release, temperature evolution, compressive strength, setting time, and microstructure, this study seeks to establish a reliable performance basis for further development of high-performance PA/MPC composites with controllable heat release.

2. Materials and Methods

2.1. Materials

Dead burned MgO was provided by Yingkou Magnesite Chemical Group Co., Ltd., Dashiqiao, China with an MgO content of 92% (Table 1). Potassium dihydrogen phosphate (KH_2PO_4, AR grade, 99.5% purity) and borax ($Na_2B_4O_7{\cdot}10H_2O$, AR grade, 99.5% purity) were provided by Shanghai Aladdin Biochemical Technology Co., Ltd., Shanghai, China. PAs with different phase change temperatures, including n-Octadecane (n-C18), n-Eicosane (n-C20), and n-Docosane (n-C22) were provided by Hebei Ruosen Technology Co., Ltd., Shijiazhuang, China. Their phase change temperatures and latent heats were characterized

by differential scanning calorimeter (DSC, NETZSCH 3500, NETZSCH-Gerätebau GmbH, Selb, Germany) under N_2 atmosphere, with detailed results presented in Table 2. MPC specimens were prepared according to a specific mix design, designated as Blank; the mass ratio of dead burned MgO to KH_2PO_4 was 4:1, and borax was added at 8% of the mass of dead burned MgO, as shown in Table 3. The PA content in the PA/MPC composites was calculated as a mass fraction of the total MPC mass, with a gradient of 2%, 4%, 6%, and 8%. The resulting PA/MPC specimens were designated as C-18-2, C-18-4, C-18-6, C-18-8, C-20-2, C-20-4, C-20-6, C-20-8, C-22-2, C-22-4, C-22-6, and C-22-8.

Table 1. Main chemical component of dead burned MgO.

Oxide	MgO	SiO_2	CaO	Fe_2O_3	IL
Content/%	92.00	4.50	2.00	1.20	0.30

Table 2. Phase change point and latent heat of PAs.

PA	Phase Change Point/°C	Latent Heat/(J/g)
n-C18	34.22	197.30
n-C20	39.92	216.00
n-C22	49.00	238.40

Table 3. Mix designs of MPC in this study referring to 100 g of dead burned MgO + KH_2PO_4.

Specimen No.	n-C18/%	n-C20/%	n-C22/%	Dead Burned MgO/g	KH_2PO_4/g	Borax/g	w/c
Blank	-	-	-	80.00	20.00	6.40	0.16
C-18-2	2.00	-	-	80.00	20.00	6.40	0.16
C-18-4	4.00	-	-	80.00	20.00	6.40	0.16
C-18-6	6.00	-	-	80.00	20.00	6.40	0.16
C-18-8	8.00	-	-	80.00	20.00	6.40	0.16
C-20-2	-	2.00	-	80.00	20.00	6.40	0.16
C-20-4	-	4.00	-	80.00	20.00	6.40	0.16
C-20-6	-	6.00	-	80.00	20.00	6.40	0.16
C-20-8	-	8.00	-	80.00	20.00	6.40	0.16
C-22-2	-	-	2.00	80.00	20.00	6.40	0.16
C-22-4	-	-	4.00	80.00	20.00	6.40	0.16
C-22-6	-	-	6.00	80.00	20.00	6.40	0.16
C-22-8	-	-	8.00	80.00	20.00	6.40	0.16

The contents of n-C18, n-C20 and n-C22 are calculated by the mass fraction of total MPC mass (dead burned MgO + KH_2PO_4 + borax). The borax content is set at 8% of the mass of dead burned MgO.

2.2. Test Specimens

Test specimens were prepared in the following steps (Figure 1). Raw materials were weighed according to the mix design in Table 3 and the specified PA content. To address the poor dispersibility and uniformity of solid PA particles in MPC mixtures at room temperature, solid PA was preheated above its phase change point to completely convert into a liquid state, ensuring sufficient fluidity for uniform blending. First, the dead burned MgO, KH_2PO_4 and borax were placed into a mixing pot, and slow mixing was started; immediately afterward, the preheated liquid PA was added slowly into the mixing pot. The four raw materials were mixed at a slow speed of 140 ± 5 r/min for 30 s to ensure uniform blending. Water was then added, followed by slow mixing for 30 s at 140 ± 5 r/min and rapid mixing for 90 s at 285 ± 10 r/min. The freshly mixed MPC mortar paste was cast

into 40 mm × 40 mm × 40 mm plastic cubic molds (triplicate specimens per group). The specimens were demolded after 1 h and then placed under standard curing conditions (20 ± 2 °C) and relative humidity > 50% until the specified ages (1 h, 3 h, 7 h, 12 h, 1 d, 3 d, 7 d, 28 d) for subsequent testing.

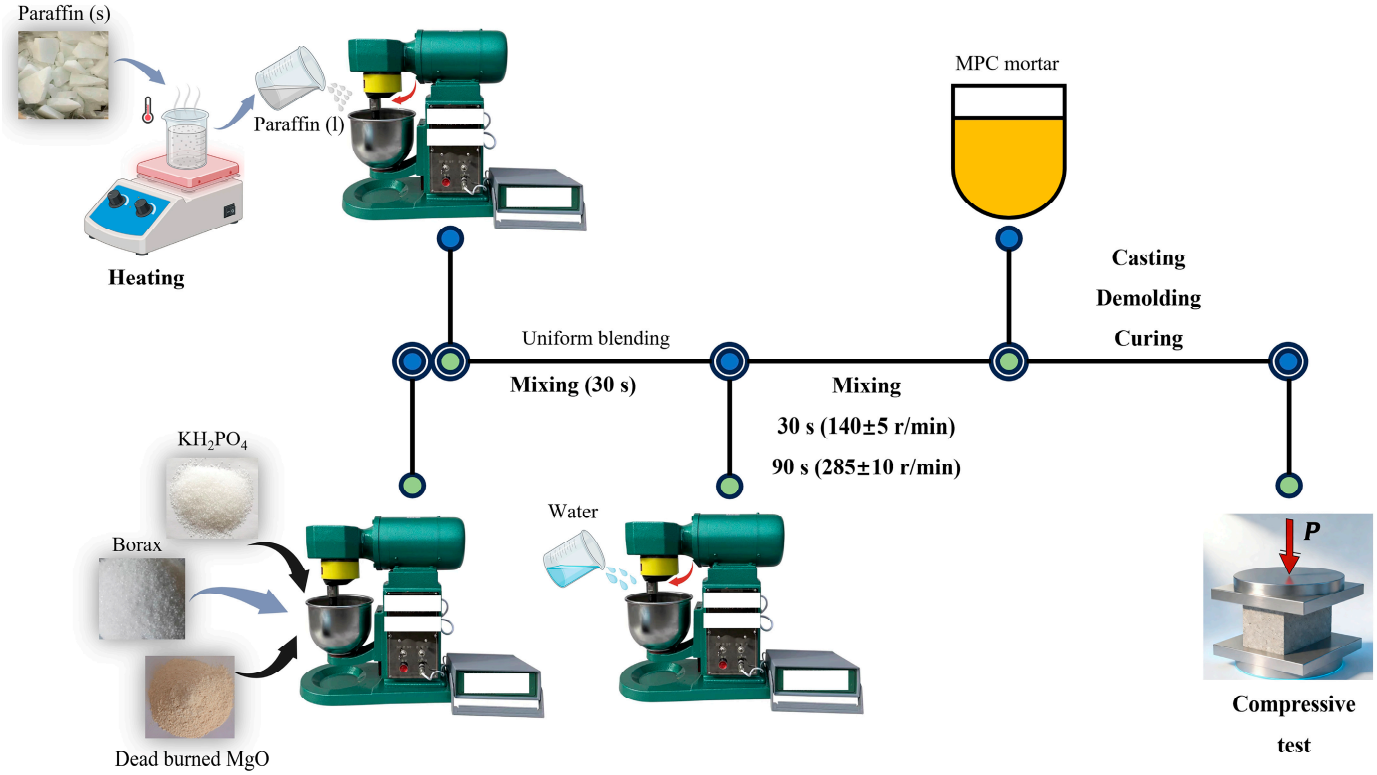


Figure 1. Preparation process of test specimens.

2.3. Test Set-Up

The thermal behaviour of the MPC specimens was characterized using a differential scanning calorimeter (DSC, NETZSCH 3500, NETZSCH-Gerätebau GmbH, Selb, Germany) under N_2 atmosphere, with a temperature range of −20 to 90 °C, and at a heating rate of 5 °C/min. The hydration heat release rate and cumulative heat of hydration of MPC were determined using TAM Air 8-Channel Standard Volume Calorimeter at 20 °C (TAM Air, TA Instruments, New Castle, DE, USA); the water-to-cement ratio (w/c) was adjusted to 0.3 to ensure sufficient hydration. The internal temperature changes in the MPC paste specimens were monitored using a temperature recorder (RC-4HC Temperature and Humidity Data Logger, Jiangsu Elitech Electronics Co., Ltd., Xuzhou, China) with a data acquisition interval of 10 s. The compressive strength at specified ages for 40 mm × 40 mm × 40 mm cube specimens was tested using a universal testing machine (YAW-3000, Jinan Zhongluchang Testing Machine Manufacturing Co., Ltd., Jinan, China). The loading rate was 0.6 kN/s, with three specimens tested per group and results averaged. The setting time of the MPC mortar was determined using a Vicat apparatus (Beijing Zhongke Luda Testing Instrument Co., Ltd., Beijing, China) in accordance with the standard Test Methods for Water Requirement of Standard Consistency, Setting Time and Soundness of the Portland Cement (GB/T 1346-2024) [44]. Given the rapid setting of MPC, the initial setting time was taken as the setting time. The phase composition of the MPC paste specimens was analysed using an X-ray diffractometer (XRD-6100, Shimadzu Corporation, Kyoto, Japan) with Cu Kα radiation (λ = 0.15406 nm) operating in the Bragg–Brentano geometry, at a scanning speed of 2°/min and a scanning range of 10–70°. The microstructure of the MPC

specimens was observed using a field emission scanning electron microscope (FE-SEM, MLA650F, Thermo Fisher Scientific Inc., Waltham, MA, USA).

3. Results and Discussion

3.1. Phase Change Performance Analysis of PA/MPC

Figure 2 shows the DSC heating curves of MPC, PAs, and PA/MPC specimens with different PA contents. As shown in Figure 2a, the DSC curve of MPC remained stable over the tested temperature range, with no endothermic or exothermic phenomena observed. In contrast, all three PAs (n-C18, n-C20, and n-C22) exhibited distinct endothermic peaks, with their phase change temperatures and latent heats showing a positive correlation with carbon chain length. After incorporating PA, the DSC curves of PA/MPC still retained pronounced endothermic peaks (Figure 2b–d). At the same PA content, the phase change temperature and latent heat of PA/MPC also followed the order n-C22/MPC > n-C20/MPC > n-C18/MPC. As the PA content increased from 2% to 8%, the latent heat of PA/MPC rose progressively, reaching a maximum of 14.68 J/g at an n-C22 content of 8%. These results verify the successful integration of PAs into MPC and provide a thermal basis for interpreting subsequent hydration heat regulation efficacy.

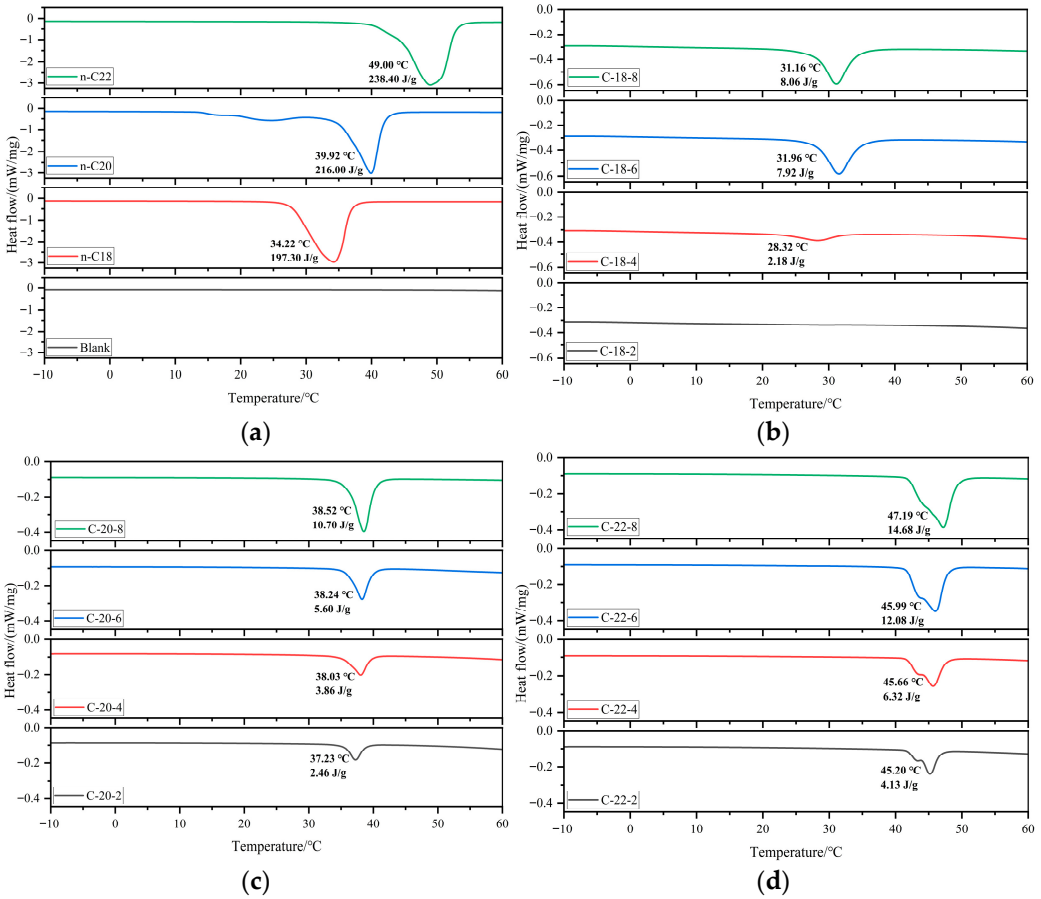


Figure 2. DSC curves of MPC with different PA contents: (**a**) MPC and PAs; (**b**) n-C18/MPC; (**c**) n-C20/MPC; (**d**) n-C22/MPC.

3.2. Influence of PAs on MPC Hydration Temperature Rise

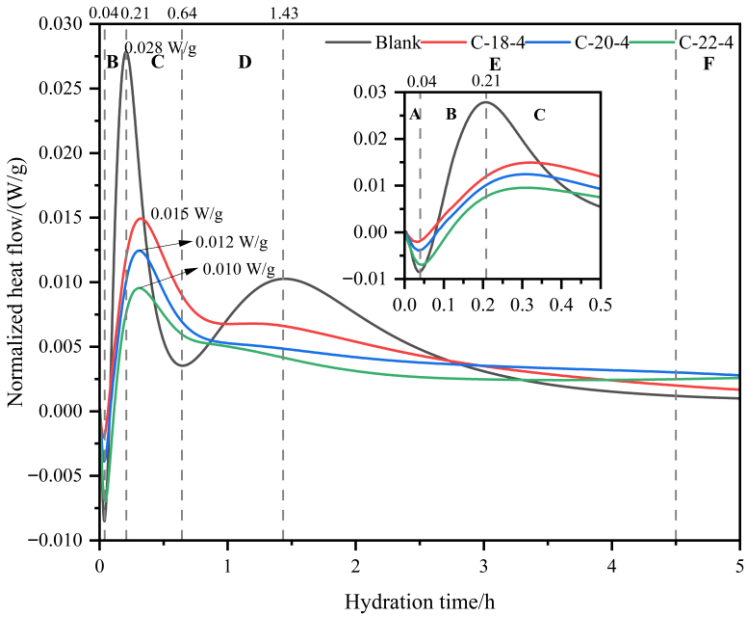
3.2.1. Changes in MPC Hydration Heat Release

Figure 3 presents the curves of hydration heat release rate and cumulative heat release for MPC and PA/MPC specimens containing 4% PA with different phase change temperatures. The hydration heat release process of MPC consisted of one endothermic

stage followed by two exothermic stages (Figure 3), corresponding to the endothermic dissolution of KH_2PO_4, the exothermic dissolution of MgO, and the exothermic formation of hydration products such as $KMgPO_4 \cdot 6H_2O$ [34,45,46]. Based on existing classification methods for hydration heat release stages, six distinct stages (A–F) were identified [47,48], as detailed below:

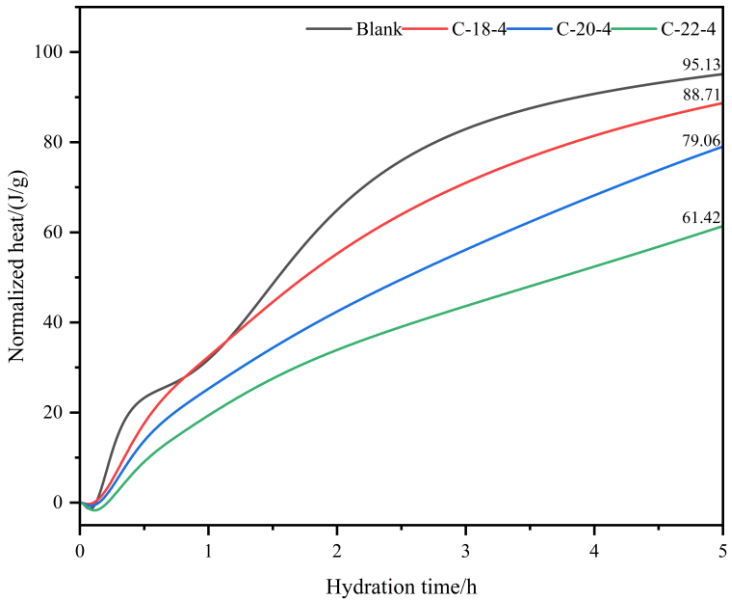
- **Stage A**: Lasting approximately 2.4 min (0.04 h), MPC absorbed heat from the environment at an increasing rate after water addition. This stage was dominated by the dissolution of KH_2PO_4 and concluded upon reaching the endothermic trough.
- **Stage B**: The heat release rate of MPC increased rapidly, marking the transition from endothermic to exothermic hydration. MgO dissolution dominated this stage, which concluded after approximately 0.21 h, reaching the first exothermic peak (0.028 W/g).
- **Stage C**: MPC continued to release heat, but the rate decreased rapidly, reaching a trough point at approximately 0.64 h.
- **Stage D**: The heat release rate of MPC increased again, dominated by the formation of hydration products like $KMgPO_4 \cdot 6H_2O$. This stage ended at approximately 1.43 h, reaching the second exothermic peak.
- **Stage E**: The heat release rate of MPC gradually decreased as the hydration process progressively stabilized.
- **Stage F**: This stage started approximately 4.5 h after hydration commenced, characterized by a stable hydration process of MPC with no further change in heat release rate.

The incorporation of n-C18, n-C20, and n-C22 significantly altered the hydration process of MPC, resulting in a slowdown of heat release and a reduction in the exothermic peak. As shown in Figure 3a, the first exothermic peak in Stage B was significantly delayed and its intensity decreased from 0.028 W/g (MPC) to 0.015 W/g, 0.012 W/g, and 0.010 W/g for n-C18, n-C20, and n-C22 composites, respectively. The second exothermic peak in Stage D disappeared, and the overall hydration heat release process was retarded. Furthermore, as indicated in Figure 3b, the cumulative heat release of MPC at 5 h was 95.13 J/g, while that of PA/MPC with n-C18, n-C20, and n-C22 decreased to 88.71 J/g, 79.06 J/g, and 61.42 J/g, respectively.



(**a**)

Figure 3. *Cont.*



(**b**)

Figure 3. Characteristic hydration heat release curve of MPC: (**a**) Normalized heat flow of MPC, with the inset showing a magnified view of the hydration process stages A, B, and C; (**b**) Normalized heat of MPC.

To further evaluate the effect of PA in regulating the hydration heat release process of MPC, a comparison with other reported additives is summarized in Table 4. As indicated, the three PAs reduced the first exothermic peak by 46–64%, outperforming many common additives such as bauxite tailings (22%), $Zn(NO_3)_2$ (19%), and $CaCl_2{\cdot}6H_2O$ (19%), and matching or exceeding the effectiveness of $Na_2SO_4{\cdot}10H_2O$ (42%) and a $Ca(NO_3)_2{\cdot}4H_2O/Na_2SO_4{\cdot}10H_2O$ blend (50%).

Table 4. Comparison of hydration exothermic peak regulation to other studies.

Additives	M/P	*w/c*	Original Exothermic Peak/(W/g)	Exothermic Peak/(W/g)	Decrease/%	Ref.
C-18	4:1 [a]	0.16	0.028	0.015	46	-
C-20	4:1 [a]	0.16	0.028	0.012	57	-
C-22	4:1 [a]	0.16	0.028	0.010	64	-
$Na_2SO_4{\cdot}10H_2O$	4:1 [a]	0.12	0.0269	0.0156	42	[38]
Bauxite tailings (BTs)	7:2 [a]	0.16	0.0082	0.0064	22	[49]
$Zn(NO_3)_2$	4:1 [b]	1	0.0440	0.0355	19	[50]
$CaCl_2{\cdot}6H_2O$	9:2 [b]	0.14	0.0094	0.0076	19	[33]
$Ca(NO_3)_2{\cdot}4H_2O/Na_2SO_4{\cdot}10H_2O$	3:1 [a]	0.12	0.022	0.011	50	[34]

[a] is the weight ratio; [b] is the mole ratio.

These results systematically demonstrate that PA incorporation effectively delays MPC hydration heat release. The regulation effect strengthened with increasing PA phase change temperature and latent heat, following n-C22 > n-C20 > n-C18, which can be explained by the greater heat absorption capacity of higher-temperature PAs during phase change. This thermal buffering action lowers the internal temperature rise of the MPC matrix, thereby slowing the dissolution of MgO and the subsequent formation of hydration products [36].

3.2.2. Temperature Rise Variations in PA/MPC Systems

Figure 4 shows the temperature rise curves and peak hydration temperature variations for the three PA/MPC systems at different PA contents. The peak hydration temperature of MPC was 56.50 °C, occurring at 27.67 min (Figure 4b). For PA/MPC incorporating PA with higher phase change temperature, the peak hydration temperature gradually decreased with increasing PA contents, while the time to reach the peak temperature exhibited a delayed trend. As shown in Figure 4c, when the n-C20 content increased from 2% to 8%, the peak hydration temperature of PA/MPC decreased sequentially from 56.50 °C to 49.40 °C, 47.30 °C, 46.20 °C, and 45.30 °C. After incorporating n-C22, the reduction in peak hydration temperature was more pronounced, and the arrival time consistently delayed compared to MPC (Figure 4e,f). Although the incorporation of n-C18 also reduced the peak hydration temperature of MPC, the extent of reduction first intensified and then weakened with increasing content (Figure 4a,b). Regarding the time to reach the peak temperature, the incorporation of 6% and 8% n-C18 actually shortened, rather than prolonged.

A comparative analysis with other MPC additives reported in the literature further highlights the effect of PA in regulating the hydration temperature (Table 5). The three PAs lowered the peak hydration temperature by approximately 15–16%, outperforming several other materials reported in the literature, such as AEA/MPCM (6%), $Na_2SO_4 \cdot 10H_2O$ (3%), red mud (6%), and steel slag powder (9%), and performing comparably to metakaolin, Al_2O_3 (16%), K_2HPO_4 (16%), and fly ash (17%).

Table 5. Comparison of hydration peak temperature regulation to other studies.

Additives	M/P [a]	*w/c*	Original T_{peak}/°C	T_{peak}/°C	Decrease/%	Ref.
C-18	4:1	0.16	56.5	48.3	15	-
C-20	4:1	0.16	56.5	47.3	16	-
C-22	4:1	0.16	56.5	48.2	15	-
AEA/MPCM	3:2	0.34	39.0	36.5	6	[51]
$Na_2SO_4 \cdot 10H_2O$	4:1	0.12	62.7	61.0	3	[38]
Gold mine tailing (GT)	7:5	0.17	50.6	43.5	14	[52]
Red mud	3:1	0.18	65.3	61.7	6	[53]
Metakaolin (MK)	3:1	0.09	42.8	35.8	16	[54]
Al_2O_3	3:1	0.09	42.8	36.0	16	[54]
K_2HPO_4	9:2	0.12	62.5	52.5	16	[55]
Broax	9:2	0.12	62.5	60.0	4	[55]
Fly ash (FA)	9:2	0.15	42.0	35.0	17	[56]
Steel slag powder	3:1	0.108	48.0	43.5	9	[57]
$Ca(NO_3)_2 \cdot 4H_2O/Na_2SO_4 \cdot 10H_2O$	3:1	0.12	61.5	52.9	14	[34]

[a] is the weight ratio; T_{peak} is the peak hydration temperature of MPC; AEA is Air Entraining Additive, Centrament Air 207 from MC-Bauchemie Müller GmbH & Co. KG, Bottrop, Germany; MPCM is Microencapsulated Phase Change Materials, Micronal® DS 5008X from BASF SE, Ludwigshafen, Germany.

The incorporation of n-C18, n-C20, and n-C22 also introduced temperature plateaus during the heating and cooling process of MPC, occurring at 27.5 °C, 35 °C, and 42.5 °C, close to the phase change temperatures of the three PAs. This corresponds to the heat storage and release process of the PA within the PA/MPC system. As the PA content increased, the duration of the plateau extended, indicating an enhanced temperature regulation capability.

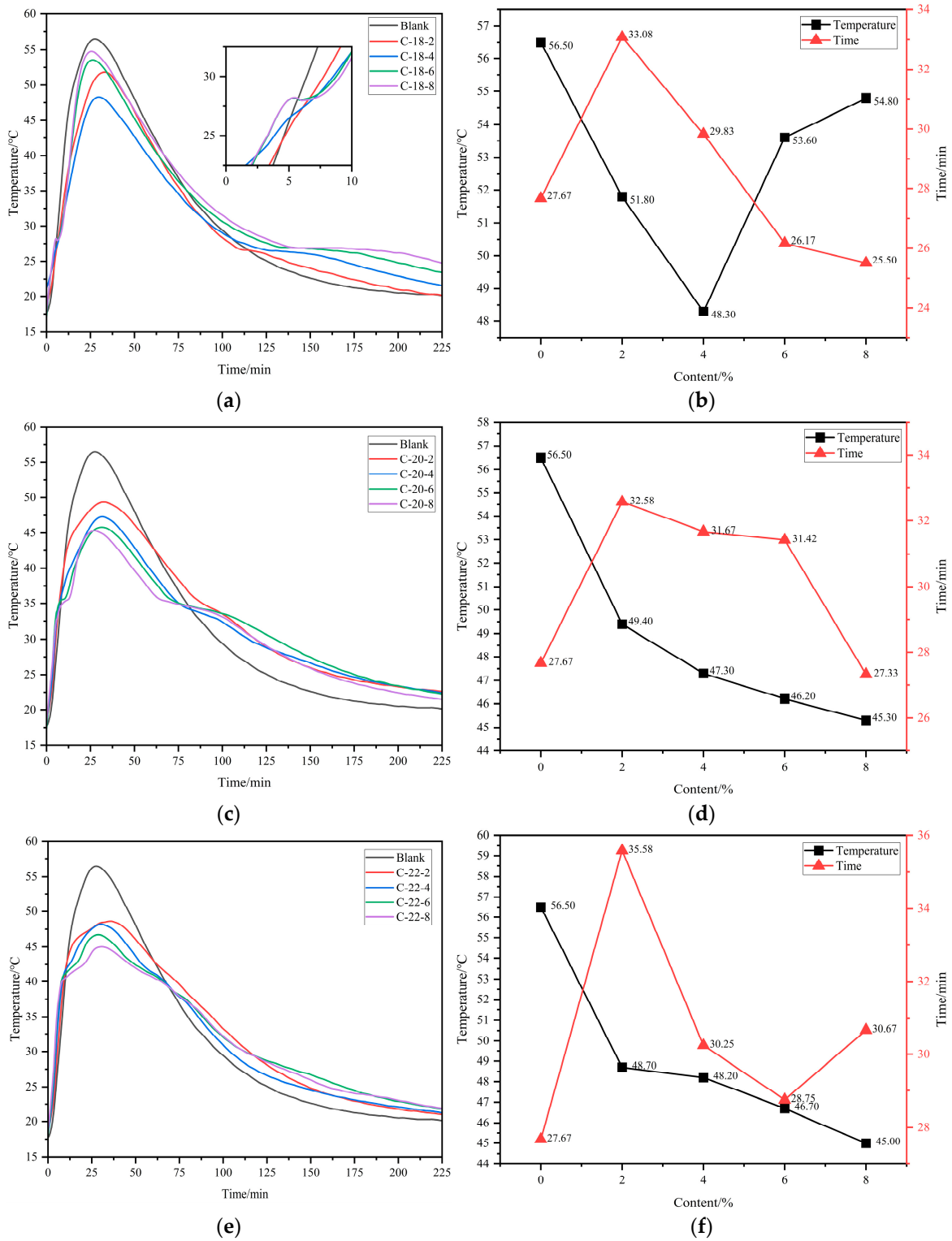


Figure 4. Temperature rise variation of MPC with different PA contents: (**a**) Temperature rise of n-C18/MPC, with the inset showing a magnified view of the temperature platform; (**b**) Peak temperature and corresponding time of MPC with different n-C18 contents; (**c**) Temperature rise of n-C20/MPC; (**d**) Peak temperature and corresponding time of MPC with different n-C20 contents; (**e**) Temperature rise of n-C22/MPC; (**f**) Peak temperature and corresponding time of MPC with different n-C22 contents.

Collectively, these findings demonstrate that PA incorporation offers an effective strategy for controlling the hydration temperature rise in MPC, highlighting positive

significance for suppressing thermal cracks in MPC and holding potential value for thermal insulation applications [8,11,12,14,22,26].

3.3. Influence of PAs on the Compressive Strength of MPC

The development of compressive strength in PA/MPC composites was found to exhibit a defined trade-off against the achieved hydration heat regulation. As illustrated in Figure 5, the compressive strength varied with PA type and content across all curing ages. Early strength of PA/MPC still maintained rapid development, exceeding 6.62 MPa at 1 h and 13.90 MPa at 7 h even for the C-20-8 mixture, but the development of strength decelerated after 1 d. The 28 d compressive strength gradually decreased with increasing PA content, with the maximum value observed at 42.96 MPa for C-18-2. This trend culminated in a pronounced compromise at 8% PA content, where strength development of all three PA/MPCs stagnated after 1 d, with a maximum 28 d compressive strength of only 25.84 MPa (C-20-8).

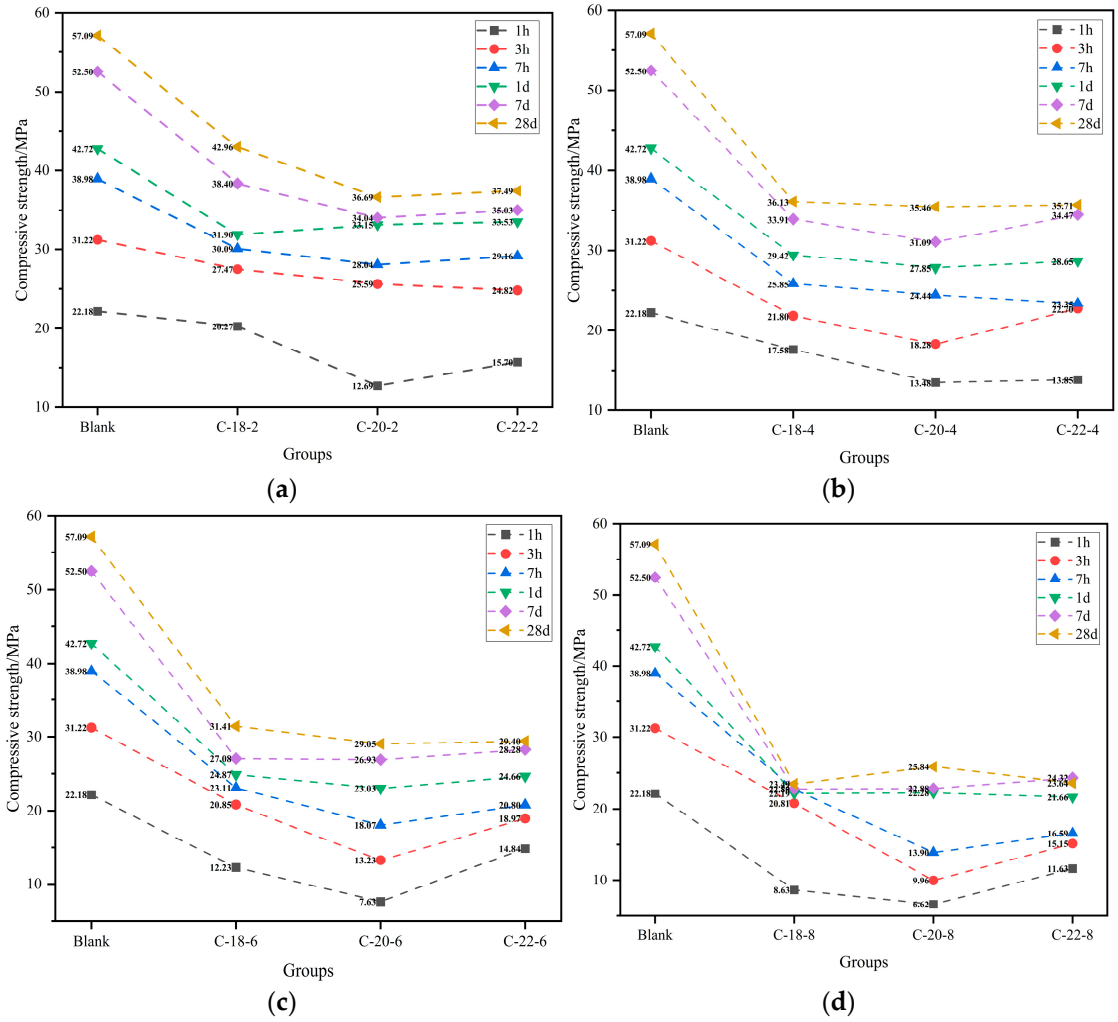


Figure 5. Compressive strength of MPC with different contents of PAs: (**a**) Contents of 2%; (**b**) Contents of 4%; (**c**) Contents of 6%; (**d**) Contents of 8%.

From a practical application standpoint, this mechanical compromise remains within acceptable limits for rapid repair. When the content of n-C18 was 8%, the 3 h compressive strength of MPC could still reach 20.81 MPa, meeting the stipulation of the industry standard Magnesium Phosphate Repair Mortar (JC/T 2537-2019) that the 3 h compressive strength should be ≥20 MPa [58]. For n-C20 and n-C22, their 3 h compressive strengths

at 2% content were 25.59 MPa and 24.82 MPa, respectively, well exceeding the standard requirements. Notably, n-C22 at 4% content still achieved a 3 h strength of 22.70 MPa, which complies with the standard; n-C20 at 4% (18.28 MPa) and n-C22 at 6% (18.97 MPa) slightly fell below 20 MPa, close to the standard requirements.

The observed mechanical compromise can be attributed to two primary reasons. First, the endothermic phase change of PA absorbed a portion of the hydration heat, thereby retarding the formation and densification of hydration products and reducing the overall hydration degree. This leads to a less dense and less interconnected microstructure, directly compromising the load-bearing capacity. Second, the dispersed PA particles introduced weak interfaces and additional pores within the matrix, which acted as stress concentration points under load, ultimately weakening the overall structural integrity of MPC.

Thus, an appropriate selection of PA type and content enables a functional balance where significant hydration heat regulation is obtained while retaining the necessary early-age mechanical properties for targeted applications. Future strategies, such as microencapsulation of PA, could be employed to mitigate this strength reduction by minimizing direct interference with the cementitious matrix.

3.4. Influence of PAs on MPC Setting Time

Figure 6 shows the influence of PA type and content on the setting time of MPC. Except for a slight increase in setting time with the incorporation of 2% n-C18, the MPC setting time generally shortened with increasing PA content. Furthermore, at the same content, the extent of reduction in setting time showed a positive correlation with PA phase change temperatures.

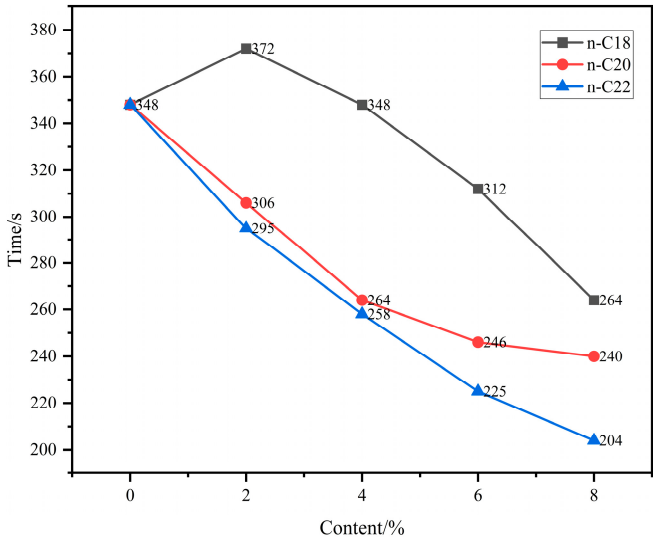


Figure 6. Setting time of MPC with different contents of PA.

This phenomenon is primarily attributed to the influence of the PA's physical state during the initial mixing stage on the mortar's flowability. During the initial mixing of MPC, low temperatures caused liquid PA to solidify rapidly upon blending with the MPC raw materials, and the exothermic heat of hydration was insufficient to melt the solidified PA. Consequently, the PA dispersed as irregular solid particles in the initial mixing stage, increasing the flow resistance of the slurry and thereby shortening the MPC setting time. Moreover, PAs with higher phase change temperatures (e.g., n-C22) exhibited a more pronounced tendency to agglomerate at lower temperatures, exerting stronger resistance to mortar flow and consequently shortening MPC setting time more significantly [59,60]. When the content of n-C18 was 2%, due to its lower phase change temperature, the heat

released during initial MPC hydration could partially melt the n-C18, resulting in a certain lubricating effect, thus exhibiting a slight retarding behaviour. This retarding effect also correlates with the absence of a distinct isothermal plateau in the heating curve of sample C-18-2 shown in Figure 4a.

3.5. Microstructural Analysis of PA/MPC

3.5.1. XRD Analysis

Figure 7 shows the XRD patterns of MPC incorporated with 4% PA at various curing ages. The results indicate that the main diffraction peaks of all samples corresponded to unreacted MgO and the primary hydration product $KMgPO_4 \cdot 6H_2O$, suggesting that the addition of PA did not alter the types of hydration products in MPC. Meanwhile, the intensity of the MgO peak in PA/MPC specimens at all ages was higher than that in MPC specimens, following the order: n-C22/MPC > n-C20/MPC > n-C18/MPC > MPC. This indicates that the incorporation of all three PAs reduced the consumption of MgO, leading to a decrease in the formation of $KMgPO_4 \cdot 6H_2O$, thus resulting in reduced hydration heat release and a lower degree of MPC hydration. This provides a reasonable explanation for the superior hydration heat regulation effect of n-C22 and the relatively minor negative impact on compressive strength observed with n-C18.

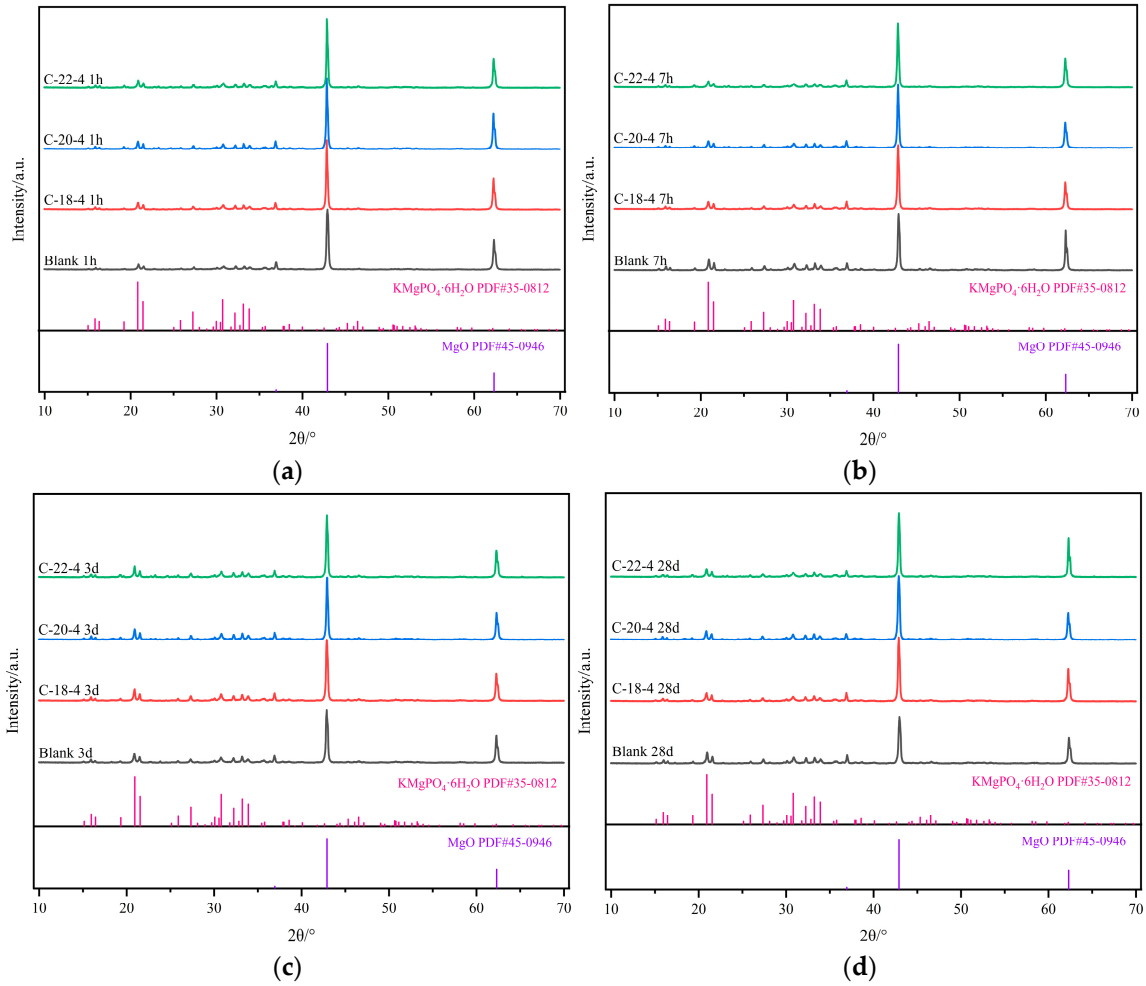


Figure 7. XRD patterns of MPC with different PA: (**a**) Curing time of 1 h; (**b**) Curing time of 7 h; (**c**) Curing time of 3 d; (**d**) Curing time of 28 d.

3.5.2. SEM Analysis

The SEM images in Figure 8 clearly reveal the influence of PA on the microstructure of MPC. As shown in Figure 8a, the MgO particles in MPC were covered with hydration products such as $KMgPO_4 \cdot 6H_2O$, with no significant exposure of the MgO matrix observed. The hydration products exhibited well-developed crystalline growth, predominantly in distinct lamellar forms that were densely interwoven, indicating a high degree of hydration and good structural integrity within MPC. In contrast, within PA/MPC specimens incorporated with the three PAs, PA particles were observed adhering to the surfaces of unhydrated MgO particles or filling pores. Meanwhile, the hydration products exhibited poorer crystallization, appearing as irregular granular structures with weak interweaving between crystals, accompanied by an increase in micro-pores and wide cracks (Figure 8b–d). This can be attributed to the endothermic phase change of PA and its physical barrier effect, which impedes contact between reactants, delaying the MPC hydration process, inhibiting the full formation of hydration products and the filling of pores. Additionally, weak interfacial zones formed between the PA and the MPC matrix can serve as initiation sites for microcracks. Collectively, the microstructural evidence confirms that PA incorporation physically hinders the nucleation, growth, and interweaving of hydration products, which disrupts microstructural continuity and compactness of MPC. These observations clearly explain the macro-scale trade-off between hydration heat regulation and macroscopic performance.

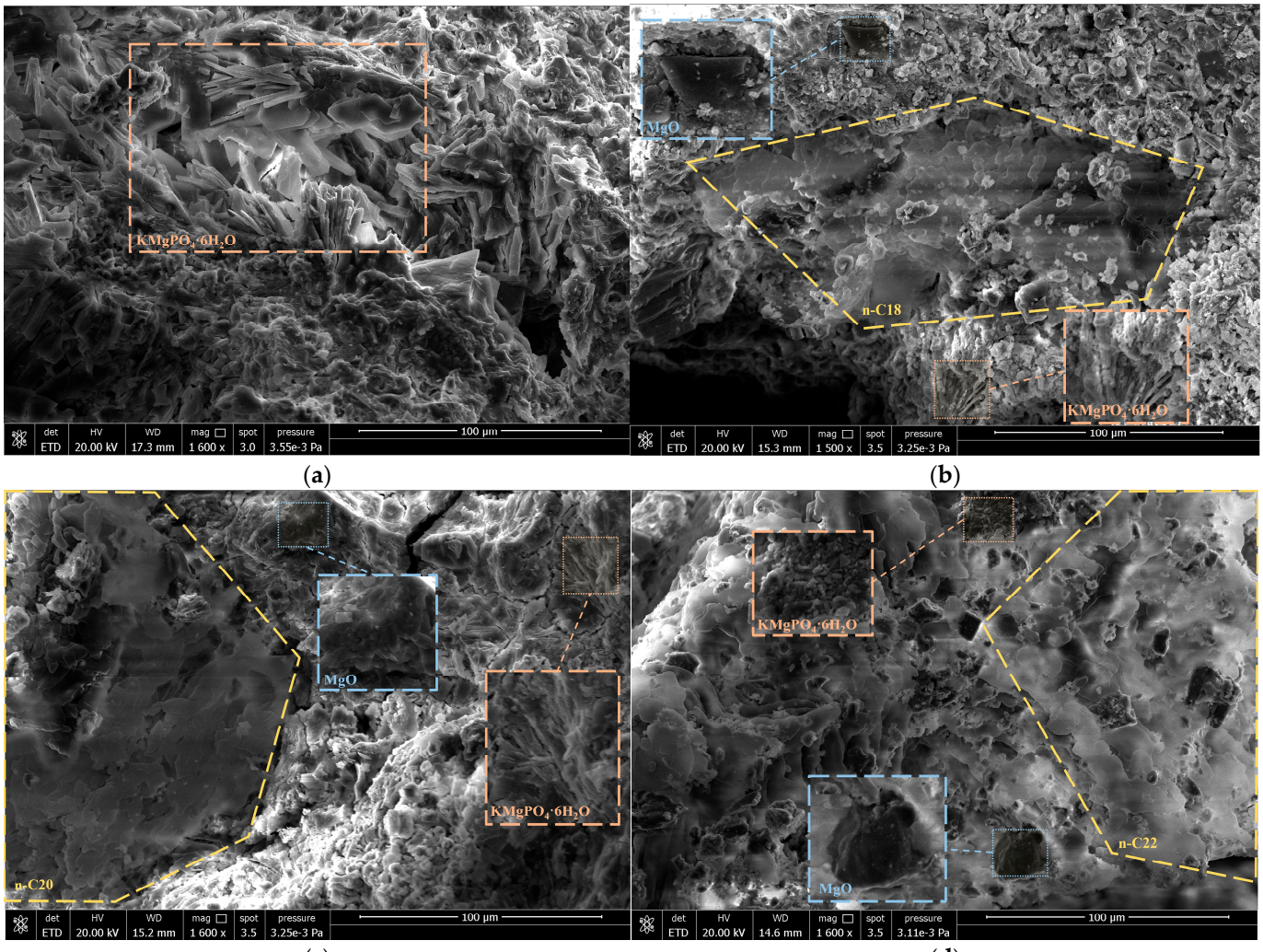


Figure 8. SEM images of MPC: (**a**) MPC (Blank); (**b**) n-C18/MPC; (**c**) n-C20/MPC; (**d**) n-C22/MPC.

4. Conclusions

Based on a systematic investigation into the phase change temperature and content of PA, this study demonstrates a clear trade-off between the MPC hydration heat regulation efficacy and overall performance. The key findings are as follows:

- The incorporation of all three PAs significantly retarded MPC hydration heat release, suppressed the internal temperature rise, and introduced stable temperature plateaus, demonstrating significant potential for mitigating thermal cracks. Specifically, 4% n-C22 achieved the optimal regulation efficacy, reducing the hydration exothermic peak by 64% and the peak temperature by 16%, outperforming many conventional MPC additives.
- As an inherent trade-off, compressive strength decreased with increasing PA content, but remained acceptable for rapid repair within specific content limits. n-C18 ($\leq$8%), n-C22 ($\leq$4%), and n-C20 (2%) all satisfied the 3 h compressive strength requirement ($\geq$20 MPa) of JC/T 2537-2019, with the highest 28 d strength (42.96 MPa) achieved by C-18-2.
- PA did not alter the types of MPC hydration products but hindered the formation and crystallization process. This reduced hydration degree and microstructure compactness, while dispersed PA particles introduced weak interfaces and pores, providing a mechanistic explanation for the observed macro-scale trade-off between hydration heat regulation efficacy and mechanical performance.

For future development, strategies such as microencapsulation of PA are highly recommended to mitigate leakage, reduce strength loss, and minimize adverse effects on setting time. Subsequent research should also include long-term durability assessment and economic feasibility analysis to fully validate the field application potential of PA/MPC composites. This study provides a fundamental basis for the rational design of MPC-based rapid repair materials with controllable hydration heat.

Author Contributions: Software, J.F.; Validation, H.Z.; Formal analysis, H.J.; Investigation, Z.L.; Resources, X.L. and Z.H.; Writing—original draft, Z.L.; Writing—review and editing, H.J., J.L. and J.F.; Visualization, X.L.; Supervision, J.L. and Z.H.; Funding acquisition, Z.L., H.Z. and Z.H. All authors have read and agreed to the published version of the manuscript.

Funding: This research was funded by the grant numbers cstc2021jcyj-msxmX0725, and the Graduate Scientific Research and Innovation Foundation of Chongqing in 2025, grant number cys25915.

Data Availability Statement: The original contributions presented in this study are included in the article. Further inquiries can be directed to the corresponding author.

Conflicts of Interest: The authors declare no conflicts of interest.

References

1. Chen, B.; Zhang, J.; Liu, A.; Zhang, L.; Xie, Z.; Ouyang, X.; Ma, Z.J. Effect of recycled oyster shell powder on hydration and strength development of magnesium phosphate cement. *Adv. Cem. Res.* **2024**, *36*, 116–128. [CrossRef]
2. Qin, Z.; Ma, C.; Zheng, Z.; Long, G.; Chen, B. Effects of metakaolin on properties and microstructure of magnesium phosphate cement. *Constr. Build. Mater.* **2020**, *234*, 117353. [CrossRef]
3. Jiang, Z.; Zhang, L.; Geng, T.; Lai, Y.; Zheng, W.; Huang, M. Study on the compressive properties of magnesium phosphate cement mixing with eco-friendly coir fiber considering fiber length. *Materials* **2020**, *13*, 3194. [CrossRef]
4. Haque, M.A.; Chen, B. Research progresses on magnesium phosphate cement: A review. *Constr. Build. Mater.* **2019**, *211*, 885–898. [CrossRef]
5. Cao, X.; Ma, R.; Zhang, Q.; Wang, W.; Liao, Q.; Sun, S.; Zhang, P.; Liu, X. The factors influencing sludge incineration residue (SIR)-based magnesium potassium phosphate cement and the solidification/stabilization characteristics and mechanisms of heavy metals. *Chemosphere* **2020**, *261*, 127789. [CrossRef] [PubMed]

6. Gardner, L.J.; Corkhill, C.L.; Walling, S.A.; Vigor, J.E.; Hyatt, N.C. Early age hydration and application of blended magnesium potassium phosphate cements for reduced corrosion of reactive metals. *Cem. Concr. Res.* **2021**, *143*, 106375. [CrossRef]
7. Deng, Q.; Lai, Z.; Yan, T.; Wu, J.; Liu, M.; Lu, Z.; Lv, S. Effect of Cr (III) on hydration, microstructure of magnesium phosphate cement, and leaching toxicity evaluation. *Environ. Sci. Pollut. Res.* **2021**, *28*, 15290–15304. [CrossRef]
8. Liu, X.; Bai, X.; He, R.; Song, X.; Luo, Q.; Wang, Z.; Cui, S. Development on Hydration Heat Controlling Materials. *Kuei Suan Jen Hsueh Pao/J. Chin. Ceram. Soc.* **2021**, *49*, 980–987. [CrossRef]
9. Walling, S.A.; Provis, J.L. Magnesia-based cements: A journey of 150 years, and cements for the future? *Chem. Rev.* **2016**, *116*, 4170–4204. [CrossRef]
10. Feijoo, J.; Álvarez-Feijoo, M.A.; Fort, R.; Arce, E.; Ergenç, D. Effects of paraffin additives, as phase change materials, on the behavior of a traditional lime mortar. *Constr. Build. Mater.* **2022**, *361*, 129734. [CrossRef]
11. Liu, J.; Yan, Y.; Li, Z.; Yang, F.; Hai, R.; Yuan, M. Investigation on the potassium magnesium phosphate cement modified by pretreated red mud: Basic properties, water resistance and hydration heat. *Constr. Build. Mater.* **2023**, *368*, 130456. [CrossRef]
12. Meng, X.; Jiang, Y.; Chen, B.; Wang, L. Research progress on the setting time and solidification mechanism of magnesium phosphate cement: A review. *Constr. Build. Mater.* **2023**, *408*, 133612. [CrossRef]
13. Zhu, Y.; Wang, Z.; Li, Z.; Yu, H. Influence of $FeCl_3 \cdot 6H_2O$ on the hydration hardening and water resistance of magnesium potassium phosphate cement. *ChemistrySelect* **2020**, *5*, 5156–5161. [CrossRef]
14. Chen, L.; Shi, Y.; Du, P.; Li, J.; Liao, P.; Du, J. Research Progress on the Preparation and Energy Storage Mechanism of Composite Phase Change Materials Based on Porous Materials Support. *J. Mater. Sci. Eng.* **2025**, *43*, 1673–2812. [CrossRef]
15. Song, J.; Xu, M.; Wang, X.; Huang, F.; Qin, G. The effects of a new phase change material on the properties of low heat cement slurries. *Drill. Fluid Complet. Fluid* **2019**, *36*, 218–223.
16. Wang, C.; Zhao, F.; Xue, Y.; Xia, D. Synthesis and performance evaluation of temperature-controlled coaggulation-promoting composite phase change endothermic agent for cementing in marine hydrate reservoirs. *Nat. Gas Ind.* **2025**, *45*, 182–192. [CrossRef]
17. Xiao, C.; Zhu, S.; Zhang, G.; Yang, X. Application Research Progress of Functional Polymers in Phase Change Thermal Storage Materials. *J. Funct. Polym.* **2021**, *34*, 336–351. [CrossRef]
18. Latibari, S.T.; Mehrali, M.; Mehrali, M.; Mahlia, T.M.I.; Metselaar, H.S.C. Synthesis, characterization and thermal properties of nanoencapsulated phase change materials via sol–gel method. *Energy* **2013**, *61*, 664–672. [CrossRef]
19. Wang, C.; Wang, L.; Wang, R.; Duan, Z.; Meng, S.; Shen, T.; Su, Q. Research progress of nano-enhanced microcapsule composite phase change materials. *Acta Mater. Compos. Sin.* **2024**, *41*, 3968–3986.
20. Sarier, N.; Onder, E. The manufacture of microencapsulated phase change materials suitable for the design of thermally enhanced fabrics. *Thermochim. Acta* **2007**, *452*, 149–160. [CrossRef]
21. Guo, S.; Wang, K.; Wang, W.; Qi, X.; Jia, Z. Preparation of binary low eutectic composite phase change microcapsule materials and their applications. *J. Mater. Eng./Cailiao Gongcheng* **2024**, *42*, 5875–5882. [CrossRef]
22. Illampas, R.; Rigopoulos, I.; Ioannou, I. Influence of microencapsulated Phase Change Materials (PCMs) on the properties of polymer modified cementitious repair mortar. *J. Build. Eng.* **2021**, *40*, 102328. [CrossRef]
23. Yin, G.; Zhang, J.; Shi, M.; Chen, W.; Zheng, X.; Wei, P.; Feng, J.; Zheng, B. Thermal properties of phase change thermal storage foam concrete. *Fuhe Cailiao Xuebao/Acta Mater. Compos. Sin.* **2023**, *40*, 4246–4259. [CrossRef]
24. Zhou, J.; Nie, Z.; Guo, Z.; Yang, J.; Zheng, Z. Review on preparation and properties of phase change concrete. *J. Jiangsu Univ. (Nat. Sci. Ed.)* **2020**, *41*, 588–595. [CrossRef]
25. Peng, Y.; Qin, Z.; Tian, Y.; Ma, G.; Chen, Q.; Qin, Y. Review of preparation and application of phase change energy storage concrete. *Concrete* **2025**, 183–188. [CrossRef]
26. Feng, Q.; Liu, X.-j.; Peng, Z.-g.; Zheng, Y.; Huo, J.-h.; Liu, H. Preparation of low hydration heat cement slurry with micro-encapsulated thermal control material. *Energy* **2019**, *187*, 116000. [CrossRef]
27. Shi, C.; Wang, P.; Yang, L. Research Progress on Modification of Paraffin-BasedPhase Change Energy Storage Materials for Construction. *Mater. China* **2022**, *41*, 607–616.
28. Bharathiraja, R.; Ramkumar, T.; Selvakumar, M.; Radhika, N. Thermal characteristics enhancement of Paraffin Wax Phase Change Material (PCM) for thermal storage applications. *Renew. Energy* **2024**, *222*, 119886. [CrossRef]
29. Xu, B.; Li, Z. Paraffin/diatomite composite phase change material incorporated cement-based composite for thermal energy storage. *Appl. Energy* **2013**, *105*, 229–237. [CrossRef]
30. Zhang, Z.; Cai, W.; Wang, L. Preparation and properties of paraffin-based composite phase change energy storage mortar. *J. Funct. Mater./Gongneng Cailiao* **2025**, *56*, 1193–1199. [CrossRef]
31. Meng, D.; Zhao, K.; Wang, A.; Wang, B. Preparation and properties of paraffin/PMMA shape-stabilized phase change material for building thermal energy storage. *J. Wuhan Univ. Technol.-Mater. Sci. Ed.* **2020**, *35*, 231–239. [CrossRef]
32. Zhang, N.; Yuan, Y. Synthesis and thermal properties of nanoencapsulation of paraffin as phase change material for latent heat thermal energy storage. *Energy Built Environ.* **2020**, *1*, 410–416. [CrossRef]

33. Li, Y.; Lin, H.; Hejazi, S.A.S.; Zhao, C.; Xie, M. The effect of low temperature phase change material of hydrated salt on the performance of magnesium phosphate cement. *Constr. Build. Mater.* **2017**, *149*, 272–278. [CrossRef]
34. Zhao, S.; Yan, H.; Zhang, H.; Wang, H.; Li, Y.; Hu, Z.; Sun, H. The effects of admixtures of inorganic hydrates on the hydration hardening of magnesium potassium phosphate cement. *Adv. Cem. Res.* **2018**, *30*, 83–92. [CrossRef]
35. Zhao, S.; Yan, H.; Wang, H.; Li, Y. Effect of Paraffin/Diatomite Form-stable Phase Change Materials on the Performances of Magnesium Potassium Phosphate Cement. *J. Logist. Eng. Univ.* **2017**, *33*, 52–57. [CrossRef]
36. Li, Y.; Yan, H.; Wang, H.; Wang, Q.; Zhao, S. Effect of paraffin/expanded graphite composite phase change materials on the hydration performances of magnesium phosphate cement. *Bull. Chin. Ceram. Soc.* **2016**, *9*, 3007–3013.
37. Li, Y.; Yan, H.; Wang, Q.; Wang, H.; Zhao, S. Effect of stearic acid composite phase change material on thermal properties of magnesium phosphate cement. *New Build. Mater.* **2017**, *44*, 122–127.
38. Zhao, S.; Yan, H.; Wang, H.; Li, Y.; Zhang, H.; Hu, Z. Influence of Na2SO4·10H2O on Hydration and Hardening of Magnesium Potassium Phosphate Cement. *Cailiao Daobao/Mater. Rev.* **2017**, *31*, 187–192+197. [CrossRef]
39. Fang, G.; Sun, P.; Yu, M.; Zhang, W.; Tan, X. Research progress in improving thermal properties of paraffin phase change materials. *Appl. Chem. Ind.* **2022**, *51*, 2433. [CrossRef]
40. Yan, T.; Chen, H. Temperature Control Performance of Paraffin Phase Change Energy Storage Module. *Packag. Eng.* **2023**, *44*, 119–125. [CrossRef]
41. Mishra, D.K.; Bhowmik, C.; Bhowmik, S.; Pandey, K.M. Property-enhanced paraffin-based composite phase change material for thermal energy storage: A review. *Environ. Sci. Pollut. Res.* **2022**, *29*, 43556–43587. [CrossRef]
42. Cunha, S.; Leite, P.; Aguiar, J. Characterization of innovative mortars with direct incorporation of phase change materials. *J. Energy Storage* **2020**, *30*, 101439. [CrossRef]
43. Cunha, S.; Lima, M.; Aguiar, J.B. Influence of adding phase change materials on the physical and mechanical properties of cement mortars. *Constr. Build. Mater.* **2016**, *127*, 1–10. [CrossRef]
44. *GB/T 1346-2024*; Test Methods for Water Requirement of Standard Consistency, Setting Time and Soundness of the Portland Cement. China Academy of Building Materials Science: Beijing, China, 2024.
45. Liu, M.; Lai, Z.; Deng, Q.; Xiao, R.; Liu, Z.; Luo, X.; Lu, Z.; Lv, S. Surface modification of magnesium oxide and its effect on the performance of magnesium phosphate cement. *Constr. Build. Mater.* **2022**, *316*, 125880. [CrossRef]
46. Viani, A.; Mácová, P. Polyamorphism and frustrated crystallization in the acid–base reaction of magnesium potassium phosphate cements. *CrystEngComm* **2018**, *20*, 4600–4613. [CrossRef]
47. Sugama, T.; Kukacka, L.E. Magnesium monophosphate cements derived from diammonium phosphate solutions. *Cem. Concr. Res.* **1983**, *13*, 407–416. [CrossRef]
48. Dai, F.; Wang, H.; Jiang, Z.; Zhao, S. Hydration Mechanism of Magnesium Phosphate Cement Based on Thermokinetics. *Cailiao Yanjiu Xuebao/Chin. J. Mater. Res.* **2018**, *32*, 247–254. [CrossRef]
49. Ruan, W.; Liao, J.; Gu, X.; Mo, J.; Cai, M.; Guo, W.; Li, F.; Zhu, Y.; Ma, X. Effects of bauxite tailings and sodium silicate on mechanical properties and hydration mechanism of magnesium phosphate cement. *Constr. Build. Mater.* **2023**, *366*, 130055. [CrossRef]
50. Lai, Z.; Lai, X.; Shi, J.; Lu, Z. Effect of Zn^{2+} on the early hydration behavior of potassium phosphate based magnesium phosphate cement. *Constr. Build. Mater.* **2016**, *129*, 70–78. [CrossRef]
51. Maldonado-Alameda, A.; Lacasta, A.; Giro-Paloma, J.; Chimenos, J.; Formosa, J. Physical, thermal and mechanical study of MPC formulated with LG-MgO incorporating Phase Change Materials as admixture. *IOP Conf. Ser. Mater. Sci. Eng.* **2017**, *251*, 012024. [CrossRef]
52. Zhu, Y.; Wang, Z.; Li, Z.; Yu, H. Experimental research on the utilization of gold mine tailings in magnesium potassium phosphate cement. *J. Build. Eng.* **2022**, *45*, 103313. [CrossRef]
53. Ma, S.; Zhang, Z.; Liu, X.; Li, Y.; Zeng, Q.; Zhang, W. Reuse of red mud in magnesium potassium phosphate cement: Reaction mechanism and performance optimization. *J. Build. Eng.* **2022**, *61*, 105290. [CrossRef]
54. Shi, Y.; Chen, B.; Ahmad, M.R. Effects of alumina as an effective constituent of metakaolin on properties of magnesium phosphate cements. *J. Mater. Civ. Eng.* **2019**, *31*, 04019147. [CrossRef]
55. Li, Y.; Shi, T.; Chen, B. Experimental study of dipotassium hydrogen phosphate influencing properties of magnesium phosphate cement. *J. Mater. Civ. Eng.* **2016**, *28*, 04015170. [CrossRef]
56. Xu, B.; Ma, H.; Shao, H.; Li, Z.; Lothenbach, B. Influence of fly ash on compressive strength and micro-characteristics of magnesium potassium phosphate cement mortars. *Cem. Concr. Res.* **2017**, *99*, 86–94. [CrossRef]
57. Yang, J.; Lu, J.; Wu, Q.; Xia, M.F.; Li, X. Influence of steel slag powders on the properties of MKPC paste. *Constr. Build. Mater.* **2018**, *159*, 137–146. [CrossRef]
58. *JC/T 2537-2019*; Magnesium Phosphate Repairing Mortar. Ministry of Industry and Information Technology of the People's Republic of China (MIIT): Beijing, China, 2019.

59. Wang, S.; Cheng, Q.; Gan, Y.; Li, Q.; Liu, C.; Sun, W. Effect of wax composition and shear force on wax aggregation behavior in crude oil: A molecular dynamics simulation study. *Molecules* **2022**, *27*, 4432. [CrossRef]
60. Kurniawan, M.; Ruwoldt, J.; Norrman, J.; Paso, K.G. Influence of wax inhibitor molecular weight on solution crystallization and rheology of monodisperse waxes. *Energy Fuels* **2021**, *35*, 7666–7680. [CrossRef]

Disclaimer/Publisher's Note: The statements, opinions and data contained in all publications are solely those of the individual author(s) and contributor(s) and not of MDPI and/or the editor(s). MDPI and/or the editor(s) disclaim responsibility for any injury to people or property resulting from any ideas, methods, instructions or products referred to in the content.